ORIGINAL ARTICLE

Regulation of synaptic architecture and synaptic vesicle pools by Nervous wreck at *Drosophila* Type 1b glutamatergic synapses

Joon Haeng Hur[1,2,4], Sang-Hee Lee[3,4], A-Young Kim[1,2,4] and Young Ho Koh[1,2]

Nervous wreck (Nwk), a protein that is present at Type 1 glutamatergic synapses that contains an SH3 domain and an FCH motif, is a *Drosophila* homolog of the human srGAP3/MEGAP protein, which is associated with mental retardation. Confocal microscopy revealed that circles in Nwk reticulum enclosed T-shaped active zones (T-AZs) and partially colocalized with synaptic vesicle (SV) markers and both exocytosis and endocytosis components. Results from an electron microscopic (EM) analysis showed that Nwk proteins localized at synaptic edges and in SV pools. Both the synaptic areas and the number of SVs in the readily releasable (RRPs) and reserve (RPs) SV pools in nwk^2 were significantly reduced. Synergistic, morphological phenotypes observed from $eag^1;;nwk^2$ neuromuscular junctions suggested that Nwk may regulate synaptic plasticity differently from activity-dependent Hebbian plasticity. Although the synaptic areas in $eag^1;;nwk^2$ boutons were not significantly different from those of nwk^2, the number of SVs in the RRPs was similar to those of Canton-S. In addition, three-dimensional, high-voltage EM tomographic analysis demonstrated that significantly fewer enlarged SVs were present in nwk^2 RRPs. Furthermore, Nwk formed protein complexes with *Drosophila* Synapsin and Synaptotagmin 1 (*D*Sypt1). Taken together, these findings suggest that Nwk is able to maintain synaptic architecture and both SV size and distribution at T-AZs by interacting with Synapsin and *D*Sypt1.
Experimental & Molecular Medicine (2018) **50**, e462; doi:10.1038/emm.2017.303; published online 23 March 2018

INTRODUCTION

Normal development, maintenance and plasticity of neuronal circuits and synaptic architectures are critical for proper brain functions in humans and other animals.[1,2] Defects in one or more genes involved with neuronal wirings or with synapse formation, development, differentiation, plasticity or transmission have been identified as the causes of many neurological disorders, including mental retardations,[3] Fragile X-syndrome,[4] Rett syndrome,[5] autism,[6] Angelman syndrome[7] and mild learning disability.[8] The causative mutations may induce abnormal development of neuronal connections or synaptic architectures by perturbing one or more molecular or cellular mechanisms underlying homeostatic regulatory mechanisms, Hebbian plasticity or both.[2,8] Hebbian plasticity is the idea that strengthening or weakening synaptic efficacy in neuronal circuits is mainly determined by correlated presynaptic and postsynaptic activities.[9] Increased neuronal excitabilities can strengthen neuronal circuits by increasing the sizes of synapses, and decreased neuronal activities can eliminate synaptic connections. Activity-dependent Hebbian plasticity may explain how long-term potentiation or depression is accomplished without extensive genetic instruction. Nevertheless, without a homeostatic regulatory mechanism keeping neuronal circuits from runaway excitation or quiescence, Hebbian plasticity may not be sufficient to explain how synaptic architectures and neuronal circuits in the brains maintain excitability within physiological limits during learning and development.[9-11] Homeostatic regulatory mechanisms are considered to have important roles in maintaining some consistency in neuronal properties despite the changes induced by activity-dependent Hebbian plasticity by altering preneuronal and/or postneuronal properties, such as synaptic vesicle (SV) release probability, synapse sizes, neurotransmitter receptor localization or retrograde signaling.[10,12]

Because the basic functional unit in the brain is a single synapse,[13,14] in order to understand the molecular and cellular mechanisms underlying synaptic plasticity and the molecular and cellular etiologies underlying neuronal disorders,

[1]ILSONG Institute of Life Science, Hallym University, Anyang, Republic of Korea; [2]Department of Bio-Medical Gerontology, Hallym University Graduate School, Chuncheon, Republic of Korea and [3]BioMedical Research Center, Korea Advanced Institute of Science and Technology, Daejeon, Republic of Korea
[4]JH Hur, S-H Lee and A-Y Kim contributed equally to this work.
Correspondence: Professor YH Koh, ILSONG Institute of Life Science, Hallym University, Anyang, Gyeonggi-do 431-060, Korea.
E-mail: Kohyh@hallym.ac.kr

identifying the molecular components localizes at synapses and investigating their roles *in vivo* are among the major foci in modern molecular neuro-genetics. The basic molecular components and neuronal signaling pathways in excitatory synapses in the human brains have been shown to be faithfully conserved at Type 1 glutamatergic synapses in *Drosophila* larval neuromuscular junctions (NMJs).[15–18] Therefore, the molecular and cellular mechanisms underlying synaptic plasticity have been intensively investigated in Type 1 glutamatergic synapses in *Drosophila* larval NMJs, the best-characterized synapses. A plethora of studies in *Drosophila* larval NMJs have shown that homeostatic regulatory mechanisms and Hebbian plasticity are present and actively participate in regulating the development, differentiation and plasticity of neuronal circuits and synapse architectures. Genetic alterations in neuronal activity have resulted in either increased or decreased synapse sizes in larval NMJs,[19–21] accompanied by alterations in the localization and composition of synaptic molecular components that form postsynaptic or presynaptic terminal macromolecular complexes.[22,23] Synaptic macromolecular complexes harbor synaptic scaffolding proteins, cell adhesion molecules, ion channels, various protein kinases and neurotransmitter receptors.[24] In addition, SVs are linked to active zones (including exocytosis and endocytosis machineries) by proteins regulating the trafficking of SVs from the reserve pool (RP) to readily releasable pool (RRP).[25,26] The *in vivo* functions of evolutionary conserved molecular components present at synapses were revealed by studies using available mutant alleles in *Drosophila*. Discs large (DLG), the *Drosophila* homolog of membrane-associated guanylated kinase (MAGUK) family proteins, are critical for the proper targeting and localization of Shaker type K^+ channels,[27] Ca^{2+}/calmodulin-dependent kinase II[28] and the *Drosophila* cell adhesion molecule, Fasciclin II (FasII),[29] at synapses. Mutations in various K^+ channels are resulted in increased sizes of synapses at larval NMJs, a typical example of Hebbian plasticity. In addition, hyperpolarization of muscle resting potentials via transgenic expression of inward rectifier K^+ channel Kir2.1 induced increased presynaptic release of neurotransmitters to produce normal levels of depolarization, a typical example of homeostatic regulatory mechanisms.[30] Furthermore, CaMKII and cAMP-dependent protein kinase have been shown to be involved with homeostatic regulatory mechanisms via regulating retrograde signaling that alters the physiological properties at the presynaptic terminals.

Nervous wreck (Nwk), a SRC homology 3 (SH3) domain and Fes/Cip4 homology-Bin/Amphiphysin/Rvs167 (F-Bar) domain containing protein present at Type 1 glutamatergic synapses in reticular structures, is a *Drosophila* homolog of human SLIT-ROBO Rho GTPase activating protein 3 (srGAP3)/mental disorder associated GTPase-acting protein (MEGAP), which has been linked to severe mental retardation.[3] *nwk* was identified as a negative regulator of structural and functional synaptic plasticity.[31] Key morphological phenotypes in NMJs in *nwk* loss-of-function mutants, such as increased numbers of synaptic bouton, were similar to those observed from mutations inducing increased neural activity, a classical example of Hebbian plasticity. However, the existence of other phenotypes, such as smaller synaptic boutons and synapses that were different from NMJs in hyperexcitability mutants suggested that *nwk* may not participate in canonical activity-dependent Hebbian plasticity. In this study, we provide genetic, anatomical and biochemical evidence supporting our hypothesis that 'Nwk regulates synaptic plasticity by regulating synapse architecture and maintaining SV sizes and pools'.

MATERIALS AND METHODS

Fly genetics
Flies were raised on standard *Drosophila* media at $25 \pm 1\,°C$ with 60% relative humidity. Previously characterized Canton-S (CS), *nervous wreck²* (*nwk²*), *Df(3L)Rdl2*,[31] *Fasciclin II^{e76}* (*FasII^{e76}*),[29] *ether a go-go¹* (*eag¹*) and UAS-neuronal-synaptobrevin-green fluorescence protein (n-Syb-GFP), UAS-Actin-GFP (Bloomington *Drosophila* Stock Center, Indiana University, Bloomington, IN, USA) were used in this study. *eag¹;;nwk²* and *fasII^{e76};;nwk²* double mutants were generated by recombining the first and third chromosomes.

Immunohistochemistry
Wandering-stage third-instar larvae were dissected in ice-cold Ca^{2+} free saline (128 mM NaCl, 2 mM KCl, 4 mM MgCl2, 35.5 mM sucrose, 5 mM HEPES, 1 mM EGTA, pH 7.2; Sigma-Aldrich, St Louis, MO, USA) and fixed with 4% paraformaldehyde in 0.1 M phosphate buffer (PB, pH 7.2) for 1 h at room temperature.[32] Goat anti-horseradish peroxidase (HRP)-fluorescein isothiocyanate,[33] rabbit anti-Nwk,[31] mouse monoclonal antibody (Mab)-Bruchpilot (Brp, Developmental Studies Hybridoma Bank (DSHB), University of Iowa, Iowa City, IA, USA), Mab-Fasciclin II (FasII, DSHB), Mab-Synapsin (DSHB), Mab-*Drosophila* cysteine string protein (*D*csp; DSHB), rabbit-anti-Like-clathrin adaptor protein 180 (Lap),[34] Mab-Futsch (DSHB), Mab-Neuroglian (DSHB), Mab-Highwire (Hiw, DSHB), Mab-*Drosophila* glutamate receptor IIA (DGluRIIA, DSHB), Mab-Discs larges 1 (DLG1, DSHB), Mab-*Drosophila* synaptotagmin 1 (*D*Sypt1, DSHB), rabbit anti-DAP160[35] and rabbit anti-*Drosophila* P-21 activated kinase (*D*pak) were used. Donkey anti-mouse Alexa-488 and anti-rabbit-Alexa 568 (ThermoFisher Scientific, Waltham, MA, USA) were used as secondary antibodies. The numbers of synaptic boutons on muscles 6 and 7 in the abdominal segment 2 were counted under epifluorescence microscopy. The lengths of synaptic branches and sizes of synaptic boutons were measured using measure functions in NIH Image J (Bethesda, MD, USA).[36] A Zeiss LSM700 confocal microscope (Zeiss, Oberkorchen, Germany) was used to acquire images of samples. Images were processed with the Zen (Zeiss) and Adobe Photoshop (Adobe, San Jose, CA, USA) software.

The relative intensities of anti-FasII immunoreactivity were calculated from single-slice confocal images of synaptic boutons on muscles 6 and 7 in the abdominal segment 2 processed with the anti-FasII antibody 1D4 under similar conditions. Briefly, the longitudinal axis of the synaptic boutons were decided and lines at an angle of approximately 0°, 90°, 180° and 270° from that axis were traced from the center of the synaptic bouton to the outer limit occupied by FasII immunoreactivity. Then the maximum intensity along lines (on a linear scale of 0–255) was determined using the Plot Profile function of Scion Image analysis program (version 1.62). To quantify FasII immunoreactivity at synaptic boutons, 57 synaptic boutons in *eag¹*,

83 in CS, 70 in nwk^2, 79 in nwk^2/Df or 60 in eag^1;;nwk^2 from 4 independent NMJs processed simultaneously were used for quantification. One-way analysis of variance with Tukey's *post hoc* test was performed using Excel (Microsoft, Redmond, WA, USA) to analyze the data.

Immuno-electron microscopy

Third-instar wandering-tage control and mutant larvae were dissected in ice-cold Ca^{2+}-free saline and then fixed with 0.005% glutaraldehyde and 4% paraformaldehyde in 0.1 M PB for 1 h. Body wall muscle preparations were marked and processed in the same well. After washing three times with 0.1 M PB with 0.2% Triton-X 100 (PBT), samples were incubated with rabbit anti-Nwk antibodies (diluted 1:2,000) overnight at 4 °C. After being blocked with 4% bovine serum albumin and 4% normal goat serum in 0.1 M PB, tissues were incubated with anti-rabbit-IgG conjugated to 1 nm gold (1:200 diluted; Nanoprobes.com, Yaphank, NY, USA). After washing three times with PBT, silver enhancement of nano-gold particles was performed according to the manufacturer's recommendation (Nanoprobes) for 10 min. After washing with H_2O for 5 min, samples were incubated with gold enhancement solution for 5 min. Gold enhancement was used to prevent silver deposits from etching. Silver- and gold-enhanced tissues were fixed with 1% glutaraldehyde and 4% paraformaldehyde in 0.1 M PB overnight. Tissues were washed three times with dH_2O, fixed with 1% OsO_4 in 0.1 M PB for 1 h and then dehydrated in serial EtOH and 100% Propylene-oxide (Ted Pella Inc., Redding, CA, USA). Tissues were embedded with Spurr's resin (Ted Pella Inc.) and polymerized at 60 °C overnight. The membrane-coated one-slot grids were used to collect serial thin sections (100 nm) and observed under a Jeol 1011 (Jeol Inc., Tokyo, Japan). Only Type 1b synaptic boutons on muscle 6 and 7 in the abdominal segment 2 were used for examination.

Western blot analysis

Ten wandering-stage third-instar larvae were dissected in ice-cold Ca^{2+} free saline and homogenized in ice-cold radio-immuno-precipitation assay (RIPA) buffer (150 mM NaCl, 1% IGEPAL CA-630, 0.5% Na-oxycholate, 0.1% sodium dodecyl sulfate (SDS), 50 mM Tris, pH 8.0; Sigma-Aldrich) with protease inhibitors (Halt protease inhibitor cocktail, ThermoFisher Scientific, Rockford, IL, USA). After being centrifuged at 14 000 g for 20 min at 4 °C to remove cellular debris, the amount of protein in each supernatant was determined using the BCA Protein Assay Kit (ThermoFisher Scientific, Waltham, MA, USA). A total of 20.0 µg of protein from each sample was separated on a 10% tris-glycine polyacrylamide SDS gel and then transferred to a nitrocellulose membrane (GE Healthcare Bio-Sciences AB, Uppsala, Sweden). The membranes were probed with rabbit anti-Nwk antibodies. Mouse anti-α-tubulin antibody was used as a loading control.

Coimmunoprecipitation analysis

Twenty wandering-stage third-instar larvae were dissected in ice-cold Ca^{2+} free saline and homogenized in ice-cold RIPA buffer with protease inhibitors (Halt protease inhibitor cocktail, ThermoFisher Scientific, Rockford, IL, USA). Supernatants were collected by spinning down at 14 000 g for 15 min at 4 °C. Protein A+G agarose beads (SantaCruz Biotech., San Jose, CA, USA) were blocked with RIPA buffer with 1% bovine serum albumin for 2 h with rolling at 4 °C. After being washed three times with RIPA buffer, protein A+G agarose beads were mixed with the supernatants, which contained 20 µl of

Mab-Synapsin and were rocked overnight at 4 °C. Protein A+G agarose beads were harvested by centrifugation at 14 000 g for 10 min at 4 °C, washing three times with RIPA buffer and then boiling with 1× SDS sample buffer. Proteins were separated by 10% SDS-polyacrylamide gel electrophoresis and immediately transferred onto nitrocellulose membranes. Membranes were probed with rabbit anti-Nwk, Mab-DSypt1 and Mab-Synapsin.

Transmission electron microscopy

The protocols for transmission EM and morphometric analysis of synaptic boutons have been previously published.[33] For this experiment, serial thin sections (100 nm) were collected from only Type 1b glutamatergic synaptic boutons on muscle 6 and 7 (abdominal segment 2). The thickness of thin sections was confirmed by examining wrinkles of thin sections at 15 000× with a Jeol 1011 (Jeol Inc.).

Three-dimensional tomography of synapses with high-voltage electron microscope

Thick sections (1 µm) were collected from CS and nwk^2 mutant synaptic boutons. Then 20 nm colloidal gold was applied on the surface of thick sections to create a list of fiducial points and used as a standard for determining sizes of SVs and T-shaped active zones (T-AZs). The specimens were tilted from −60° to+60° and imaged at 1° steps (121 images per view) using a high-voltage electron microscope (HVEM; Jeol) operated at 1 MV. Tilted images were aligned using the IMOD software[37] to visualize three-dimensional (3D) structures of synapses and active zones. The presynaptic and post-synaptic membranes, SVs and T-AZs were visualized. The sizes and distances of SVs from active zones were analyzed. One-way T-tests were performed by Excel (Microsoft) for statistical analyses.

RESULTS

Nwk reticulum localizes at the peri-synaptic area and SVs

The precise localization patterns of Nwk at Type I glutamatergic boutons in *Drosophila* larval NMJs were examined by performing anti-Nwk immunocytochemistry. The specificity of anti-Nwk in immunocytochemistry was confirmed by using nwk^2 null mutants (Supplementary Figure 1). Nwk signals were observed mainly at the presynaptic terminals of Type I boutons and did not overlap with DLG signals in wild-type CS NMJs (Supplementary Figure 1). DLG has been shown to be present mainly at the postsynaptic terminals of Type I boutons that have elaborated and convoluted membrane structures, named subsynaptic reticulum (SSR).[28,29] However, the outer boundaries of Nwk immuno-reactivity overlapped with anti-HRP signals, indicating neuronal membrane structures (Supplementary Figure 1)[38] and suggesting that Nwk is distributed within the presynaptic terminals of Type I boutons at the confocal microscopic level. No detectable Nwk signals were observed from NMJs or muscles of nwk^2 animals (Supplementary Figure 1C2), even though anti-DLG and anti-HRP signals appeared to be normal in nwk^2 NMJs (Supplementary Figure 1C1).

The localization patterns of Nwk at synapses in Type 1b boutons in CS were further revealed by serial double-labeling confocal microscopy employing antibodies targeting Nwk and other synaptic or cytoskeletal components (Figure 1). Nwk

4

signals, indicated in red in Figure 1, were distributed at the presynaptic terminals in reticular structures that were formed of several interlinked circles and termed Nwk reticulum. Nwk reticulum at the presynaptic terminal was observed from the surface (Figure 1b) through the center of synaptic boutons (Figures 1a and c–n). Narrow passages clear of Nwk signals are present in the middle of boutons indicated by gray arrow heads (Figure 1a and c–e). A single-slice confocal image taken from
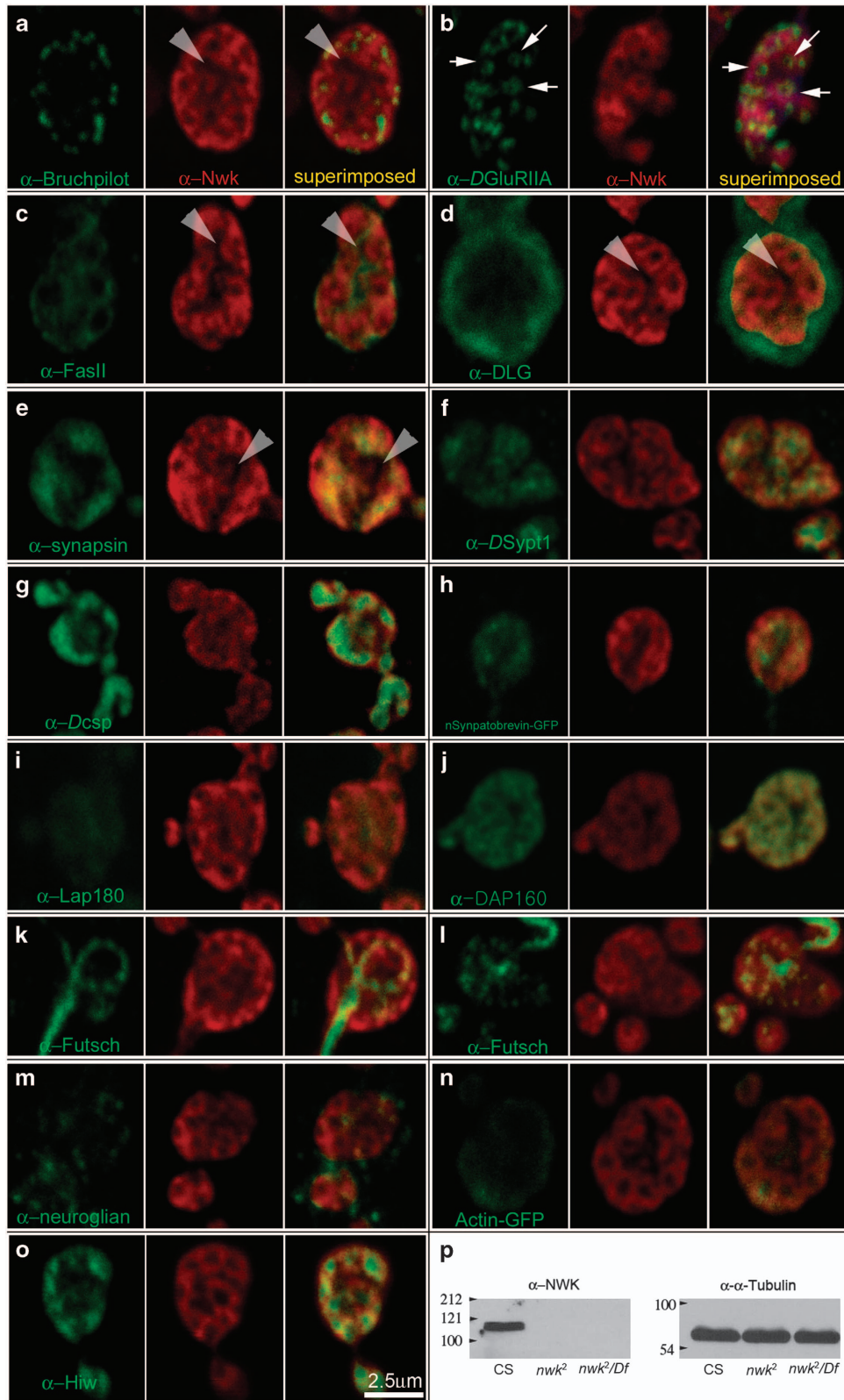
the midline of a bouton double-labeled for anti-Nwk and the T-AZ marker, Mab-Brp,[39,40] indicated that Nwk circles were present at the peri-active zones (Figure 1a). Double-labeling with a postsynaptic density maker (Mab-*D*GluRIIA)[17] showed that Nwk circles directly faced the edges of postsynaptic densities. There was a hole at the center of *D*GluRIIA signals corresponding to T-AZs (Supplementary Figure 2A) indicated by a white arrow (Figure 1b). When another postsynaptic density marker, anti-*Drosophila* p-21 activated protein kinase (*D*pak, red), was used for double-labeling with Mab-Brp (green), T-AZs were localized at the center of postsynaptic density (Supplementary Figure 2C). FasII, a *Drosophila* homolog of cell adhesion molecule has been shown to be localized on both the presynaptic and postsynaptic membranes in Type I glutamatergic NMJs.[22,29] Anti-Nwk and Mab-FasII double-labeling experiments showed that Nwk reticulum and FasII signals are not overlapped (Figure 1c). FasII signals were observed surrounding circles in the Nwk reticulum but were not present on the inner sides of Nwk circles. In addition, FasII was present at the narrow passages in the middle of synaptic boutons that were clear of Nwk signals pointed by gray arrow heads. In addition, FasII signals did not colocalize with Mab-Brp signals (Supplementary Figure 2B). These distribution patterns suggested that Nwk circles are closer to T-AZs than FasII signals at the presynaptic membranes and may regulate synapse stability. Double-labeling with a postsynaptic terminal maker (anti-DLG) showed that the Nwk reticulum was restricted to within the presynaptic terminals of Type Ib boutons (Figure 1d).

Distribution patterns of Nwk reticulum at the presynaptic terminals were further analyzed by using SV markers, such as Mab-Synapsin (Figure 1e), anti-*D*Sypt1 (Figure 1f) or Mab-*D*csp (Figure 1g); molecular components of exocytosis compartments, such as n-syb-GFP (Figure 1h), and endocytosis markers, such as anti-LAP180 (Figure 1i) and anti-Dap 160 (Figure 1j). Nwk reticulum was partially colocalized with SV markers (Figures 1e–g), n-syb-GFP signals (Figure 1h) and LAP-180 signals (Figure 1i), as indicated by the yellow colors clearly visible in the merged images. Interestingly, anti-Dap160 and anti-Nwk signals partially colocalized at Type Ib boutons (Figure 1j). Previous studies in *dap160* loss-of-function mutant showed that Nwk localizations at boutons was impaired, even though Dap160 localization at *nwk*[2] boutons was not clearly perturbed.[41]

To understand how Nwk reticulum is linked to the cytoskeleton in the presynaptic terminals, the microtubule marker Mab-Futsch (Figures 1k and l) and Actin-GFP (Figure 1m) were used to reveal cytoskeleton networks in the boutons. Presynaptic Futsch–microtubule structures traversed the synaptic boutons that were not undergoing division or sprouting (Figure 1k). However, synaptic boutons undergoing division or sprouting were usually present at the end of synaptic branches and did not have Futsch–microtubule cytoskeleton loops. Instead, Futsch–microtubule signals were diffuse and present at the center of Nwk circles, indicating that the destabilization of Futsch–microtubule loop structures is a critical process for dividing or sprouting synaptic boutons (Figure 1l).[42] These results suggested that Nwk reticulum is not directly linked to microtubules. However, Nwk reticulum at the bouton midline were partially colocalized with Actin-GFP signals, reinforcing previous reports that interactions between Nwk and the Actin cytoskeleton are important for structural and functional synaptic plasticity at the *Drosophila* larval NMJs.[31] Neuroglian, the *Drosophila* L1 homolog shown to be involved with axon pathfinding, was present on both the presynaptic and postsynaptic terminals but was not colocalized with Nwk in Type 1b boutons (Figure 1m). In addition, Nwk reticulum partially colocalized with Hiw, shown to be related with FasII-independent synaptic plasticity (Figure 1o). Western blots from larval body wall muscle extracts of CS, *nwk*[2] and *nwk*[2]/*Df* were probed sequentially with anti-Nwk or Mab-α-Tubulin (12G10) (Figure 1p). Two strong NWK bands of approximately 110 Kda that were clearly seen from CS body

---

Figure 1 Nwk reticulum at synaptic boutons in *Drosophila* larval Type 1b boutons in neuromuscular junctions (NMJs). To reveal the precise localization patterns of Nwk at the presynaptic terminals of Type 1 glutamatergic NMJs, Nwk antibodies (red) were counter-stained with antibodies targeting other identified synaptic molecular components or cytoskeleton components (green). All images are single-slice confocal images taken from a midline (a, c–n) or a surface of synaptic boutons (b). (**a**) T-AZs labeled with Mab-Brp (green) were localized at the center of circles in Nwk reticulum (red) clearly seen from a merged image. (**b**) A postsynaptic density marker, Mab-DGluRIIA (green) and anti-Nwk (red) indicated that PSDs localized at the center of circles in Nwk reticulum clearly seen in the merged image. (**c**) Mab-FasII (green) signals in a midline of synaptic bouton surrounded the Nwk reticulum (red) and localized at the Nwk-negative narrow passage indicated by white arrow heads. (**d**) Double labeling with Mab-DLG, a postsynaptic terminal structure marker (green) and anti-Nwk (red) revealed that Nwk reticulum is present at the presynaptic terminals. (**e, g, h**) Antibodies of SV proteins (green), such as Mab-synapsin(**e**), anti-*D*Sypt1 (**g**) or Mab-*D*csp2 (**h**) were present at the center of circles in Nwk reticulum (red) but not in the Nwk-negative narrow passages indicated by white arrow head. (**f**) When n-Syb-GFP was expressed using the pan-neuronal C155-Gal4 driver, n-Syb-GFP (green) was partially colocalized with Nwk reticulum (Red). (**i**) Anti-LAP180 (green) was partially colocalized with Nwk reticulum. (**j**) Mab-Hiw partially colocalized with the Nwk reticulum. Particularly strong Hiw signals were present at the center of Nwk circles (red). (**k, l**) Mab-Futsch revealed microtubules in boutons. In the stable synaptic boutons, microtubule–Futsch loops traversing the middle of synaptic boutons were clearly visible (**k**). Synaptic boutons undergoing sprouting or dividing did not have microtubule–Futsch loop structures (**l**). Instead, microtubule–Futsch signals were present at the centers of circles in NWK reticulum. (**m**) *Drosophila* L1 homolog, Neuroglian (Mab-BP104, green), did not colocalize with Nwk reticulum at the synaptic boutons. (**n**) When Actin-GFP was expressed in the neurons using C155-Gal4, Actin-GFP proteins (green) was partially colocalized with Nwk reticulum. (**o**) Nwk reticulum partially colocalized with Hiw. (**p**) A western blot from larval body wall muscle extracts of CS, *nwk*[2] and *nwk*[2]/*Df* was probed sequentially with anti-Nwk or Mab-α-Tubulin (12G10). There was no Nwk expression in *nwk*[2] and *nwk*[2]/*Df*.
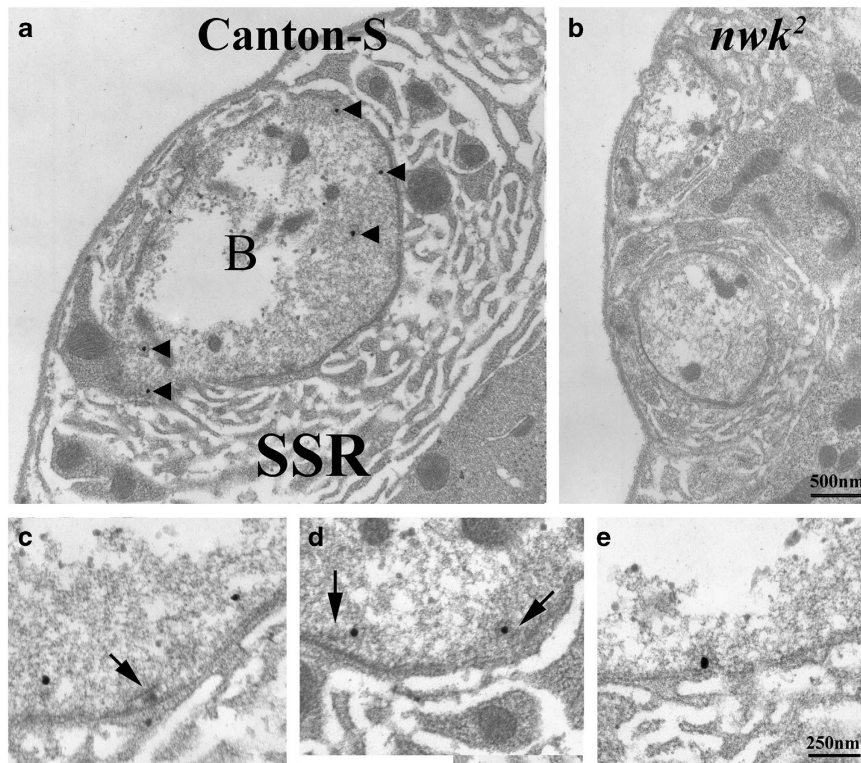
Figure 2 Nwk is localized at the edges of the synapses and in SV pools. (**a**) Anti-Nwk-positive silver- and gold-enhanced particles indicated by black arrow heads were localized at the edge of synapses or within SV pools in CS synaptic boutons. (**b**) However, no anti-Nwk-positive particles were present in nwk^2 synaptic boutons. (**c–e**) Nwk particles were localized within reserve SV pools (**c**), readily releasable SV pools (**d**) or the edge of a synapse (**e**). Black arrows indicate T-AZ at synapses. B, bouton; SSR, subsynaptic reticulum. Bar, 500 nm (**a** and **b**); 250 nm (**c–e**).

wall muscle extracts were not present in nwk^2 or nwk^2/Df body wall muscle extracts, even though similar intensities of α-Tubulin bands were detected. At least two abundant alternate splicing NWK variants are present in synapses in *Drosophila* larval NMJs. These precise and comparative localization patterns of Nwk reticulum suggest that NWK may be important for regulating synapse sizes and the trafficking of SV pools.

Localization of Nwk at synapse edges and reserve SVs were revealed by immuno-EM

Anti-Nwk immuno-EM analysis was performed to obtain further information regarding subsynaptic localization patterns of Nwk at synapses (Figure 2). Most silver- and gold-enhanced anti-Nwk particles were distributed at the edge of synapses (46.2%) or within SV pools (44.6%) in Type 1b synaptic boutons (Table 1 and Figure 2a). Two different types of SV pools at the presynaptic terminals of *Drosophila* NMJs have been suggested.[26,43,44] The SVs involved with exocytosis present near the T-AZs are called the RRP.[45] In contrast, SVs that are broadly distributed inside synaptic boutons are called the RP.[26,43,45] At the EM levels, SVs near the T-AZs were considered as RRP.[44] Therefore, the localization of Nwk particles in either the RRP or RP was further characterized. In this study, SVs present within 200 nm from the stub of T-AZs were considered to be in the RRP and were otherwise considered be in the RP. Among the 29 particles localized at the

SV pools, 5 particles were present in the RRP and 24 particles in the RP (Figures 2c–e and Table 1). Synaptic terminals of Type Ib boutons in nwk^2 NMJs processed simultaneously with CS NMJs showed significantly reduced numbers of NWK particles (Figure 2b). Even though three times more thin sections obtained from nwk^2 NMJs than those of CS NMJs were examined, only three Nwk particles were observed at the presynaptic terminals and five particles at the postsynaptic terminals or muscles (Table 1). These immuno-EM results reinforced the subsynaptic distribution patterns of NWK at the edge of synapses and SV pools and suggesting possible roles of NWK in regulating synapse stability and transmission.

Synergistic phenotypes in the bouton numbers and branch extension in eag[1];;nwk[2] NMJs

Consistent with localization patterns of Nwk at the presynaptic terminals of Type 1 glutamtergic NMJs, several morphological phenotypes, including increased numbers of synaptic boutons, extended length of synaptic branches and reduced sizes of synaptic bouton area, were observed from nwk^2 null mutant NMJs when those phenotypes from CS NMJs were compared (Figures 3a1,3b1 and 3l–3k). The numbers of synaptic boutons in nwk^2 NMJs were significantly increased compared with those in CS NMJs (CS, 112.0 ± 3.27; nwk^2, 148.2 ± 3.22; nwk^2/Df, 150.1 ± 4.63) (Figure 3i). The increased numbers of synaptic boutons have been considered evidence of activity-dependent

Table 1 Localization of Nwk proteins at *Drosophila* Type I glutamatergic synaptic boutons

Location of Nwk particles	Canton-S boutons		nwk^2 boutons	
	No. of Nwk particles	%	No. of Nwk particles	%
Synaptic membrane	2	3.1	0	0
Edge of synapses	30	46.2	2	25.0
T-shaped active zone	1	1.5	0	0
RRP[a]	5	8.0	0	0
RP[b]	24	36.6	1	12.5
Outside synaptic boutons (muscle sarcoplasm)	3	4.6	5	62.5
Total	65	100.0	8	100.0

Abbreviations: Nwk, Nervous wreck; RP, reserve SV pool; RRP, readily releasable SV pool. Note that 22 thin sections from Canton-S boutons and 72 thin sections from nwk^2 null mutant boutons were examined.
[a]SVs localized within 200 nm from the stub of T-AZs were considered the RRP.
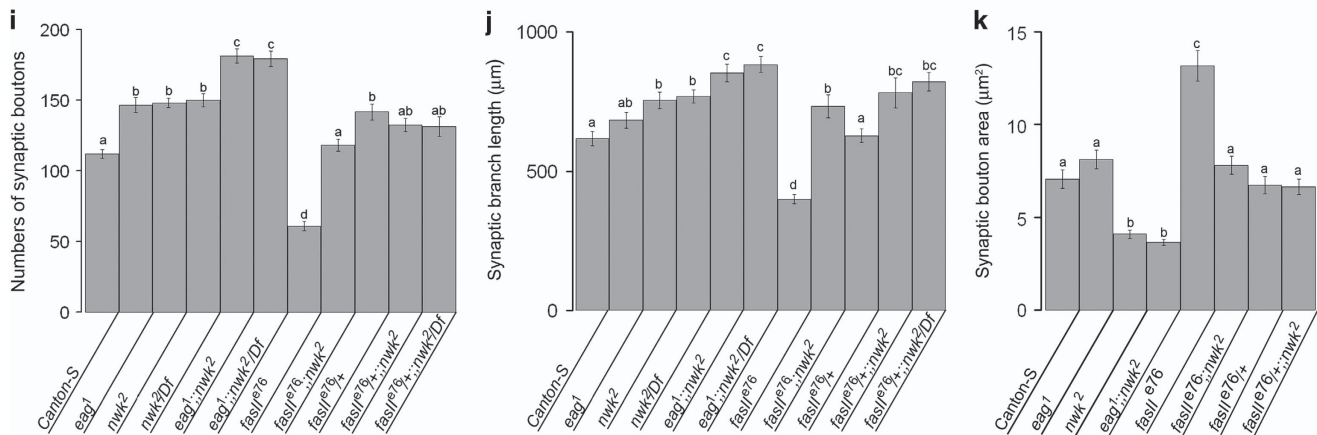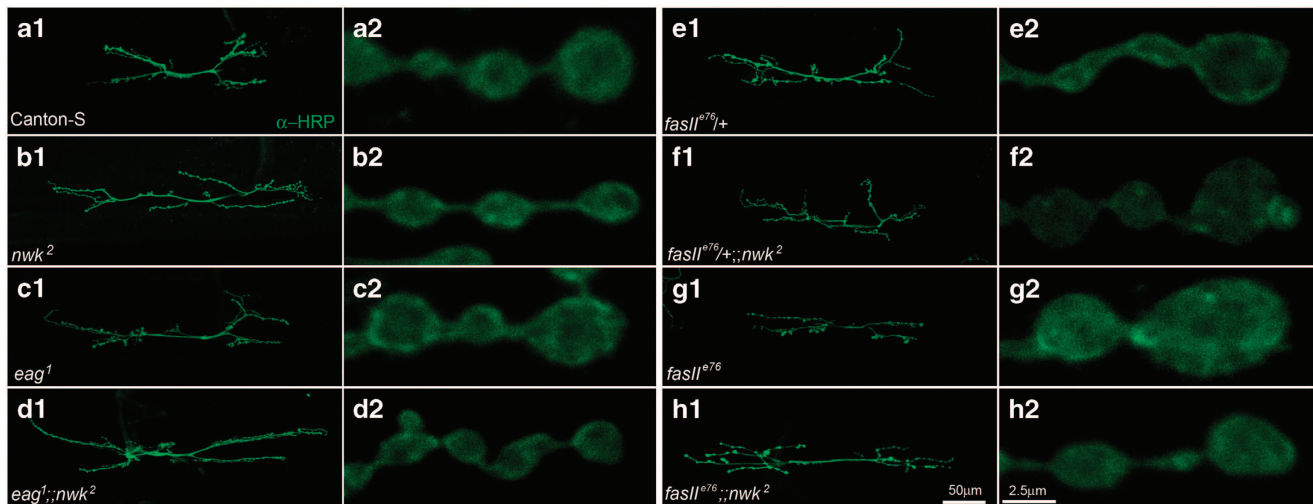[b]SVs localized farther than 200 nm from the stub of T-AZs were considered the RP.

Figure 3 Altered synaptic morphology in eag^1, $fasII^{e76}$ and nwk^2 single- or double-mutant NMJs. Gross NMJ morphologies or synaptic bouton structures of CS (**a**1 and **a**2), nwk^2 (**b**1 and **b**2), eag^1 (**c**1 and **c**2), $eag^1;;nwk^2$ (**d**1 and **d**2), $fasII^{e76}/+$ (**e**1 and **e**2), $fasII^{e76}/+;;nwk^2$ (**f**1 and **f**2), $fasII^{e76}$ (**g**1 and **g**2) and $fasII^{e76};;nwk^2$ (**h**1 and **h**2) were revealed by anti-HRP immunohistochemistry. The numbers of synaptic boutons (**i**), branch lengths (**j**) and bouton area (**k**) in eag^1, $fasII^{e76}$ and nwk^2 single- or double-mutant NMJs were compared with those of Canton-S. Characters above error bars indicate groups that are statistically identical.
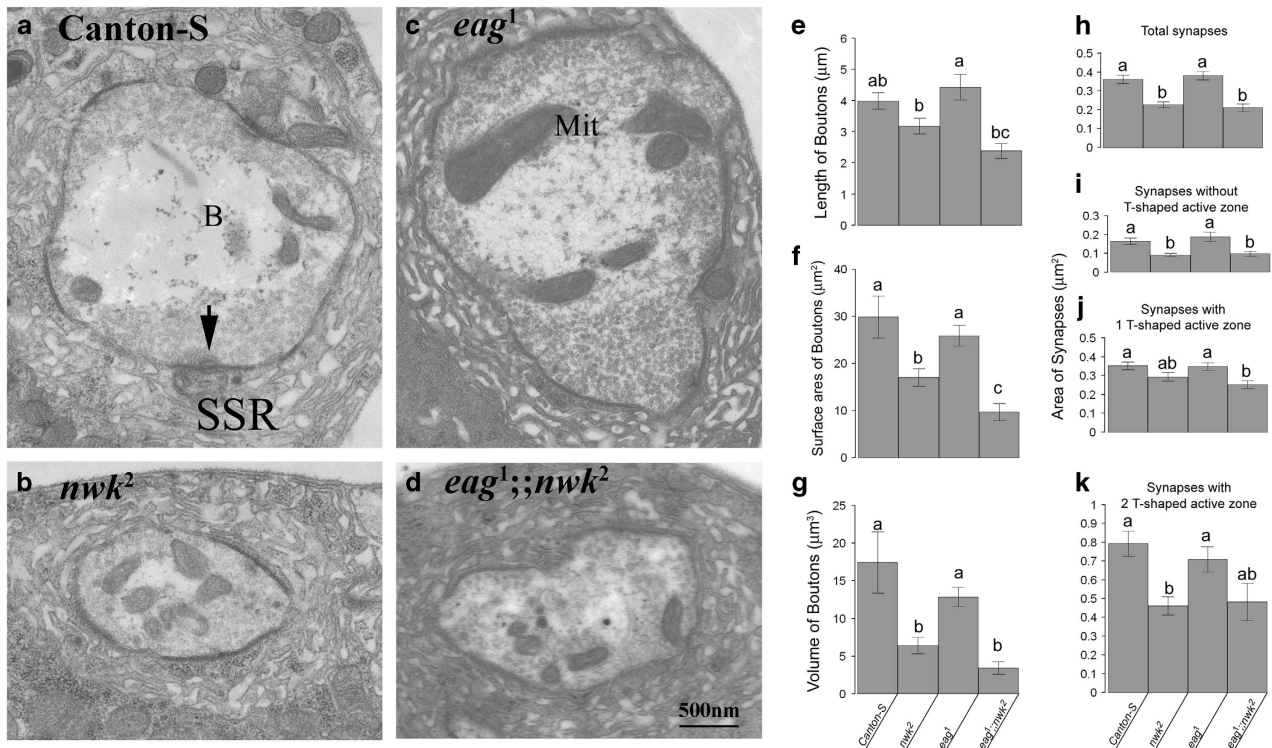
8

Figure 4 Ultrastructure of synaptic boutons in CS, nwk^2, eag^1 or $eag^1;;nwk^2$NMJs. (**a–d**) Typical transmission electron microscope images taken from midline cross-section of CS (**a**), nwk^2 (**b**), eag^1(**c**) and $eag^1;;nwk^2$ (**d**) synaptic boutons. (**e–g**) Quantification results of the length (**e**), surface area (**f**) and volume (**g**) of synaptic boutons. (**h–k**) Areas of total synapses and of synapses without (**i**), with one (**j**) or with two (**k**) T-AZs. Black arrows indicate T-AZs in synapses. B, synaptic boutons; Mit, mitochondria; SSR, subsynaptic reticulum. Characters above error bars indicate groups that are statistically identical.

Hebbian plasticity.[19] Mutations in *eag*, one of the voltage gated K+ channels, induce hyperexcitability in *Drosophila* larval NMJs (Figure 3c1). [19] The bouton number for eag^1 NMJs (146.6 ± 6) was not statistically distinguishable from that for nwk^2 NMJs but was significantly increased compared with that for CS NMJs (Figures 3b1 and i). Similar phenotypes between eag^1 and nwk^2 mutant NMJs raised possibilities that *eag* and *nwk* might be present in the same signaling pathway regulating the development of synaptic boutons. To test this possibility, $eag^1;;nwk^2$ NMJs were generated and examined (Figures 3d1 and i). $eag^1;;nwk^2$ NMJs showed significantly increased bouton numbers ($eag^1;;nwk^2$, 181.4 ± 5.06; $eag^1;;nwk^2/Df$, 179.5 ± 5.56) compared with those in eag^1or nwk^2 NMJs (Figures 3d1 and i). Synergistic phenotypes observed in $eag^1;;nwk^2$ NMJs suggested that eag^1 and nwk^2 are present in parallel or different signal transduction pathways regulating bouton numbers at Type1 glutamatergic NMJs. This notion is supported by additional morphological phenotypes observed from nwk^2 NMJs, such as elongated synaptic branches or decreased areas of boutons, that were not observed in eag^1 NMJs (Figures 3j and k). The synaptic branch lengths in nwk^2 or nwk^2/Df NMJs (nwk^2, 754.9 ± 29.9 μm; nwk^2/Df, 768.8 ± 23.8 μm) were significantly increased compared with those of CS NMJs (CS, 617.4 ± 25.1 μm). However, the synaptic branch length in eag^1 NMJs (683.3 ± 28.7 μm) was not significantly different from those of either CS or *nwk* mutant NMJs (Figure 3j). The length

of *eag* and *nwk* double-mutant NMJs ($eag^1;;nwk^2$, 852.9 ± 31.6 μm; $eag^1;;nwk^2/Df$, 882.7 ± 28.7 μm) was significantly different from that of *nwk* NMJs (Figures 3d1 and j). These results suggested that *eag* and *nwk* may not act via the same signaling mechanisms regulating the numbers of synaptic boutons and NMJ length.

Smaller synaptic boutons in nwk^2 and $eag^1;;nwk^2$ NMJs
Another morphological phenotype in nwk^2 NMJ was reduced bouton sizes. Bouton sizes in nwk^2 NMJs (4.095 ± 0.225 μm^2, $n = 124$; Figures 3b2 and k) were significantly smaller than those of CS (7.051 ± 0.499 μm^2, $n = 103$; Figures 3a2 and k) or eag^1 NMJs (8.127 ± 0.507 μm^2, $n = 103$; Figures 3c2 and k) but similar to those of $eag^1;;nwk^2$ NMJs (3.650 ± 0.154 μm^2, $n = 154$; Figures 3d2 and k). Consistently, typical transmission EM images taken from across the midlines of boutons in CS, nwk^2, eag^1 or $eag^1;;nwk^2$ NMJs showed that bouton sizes in nwk^2 or $eag^1;;nwk^2$ were significantly smaller than those in CS or eag^1 (Figures 4a–d). Further morphometric analysis by based on serial transmission EM images revealed that the average synaptic bouton length in nwk^2 NMJs (3.18 ± 0.25 μm, $n = 9$) was similar to those in CS NMJs (3.99 ± 0.26 μm, $n = 7$) but significantly smaller than those of eag^1 NMJs (4.43 ± 0.41 μm, $n = 7$; Figure 4e). The bouton surface area in nwk^2NMJs (17.04 ± 1.87 μm^2) was significantly decreased, $<70\%$ of CS (29.90 ± 4.46 μm^2) or $<60\%$ of eag^1 (25.93 ± 2.19 μm^2) (Figure 4f). The bouton volume in nwk^2 NMJs
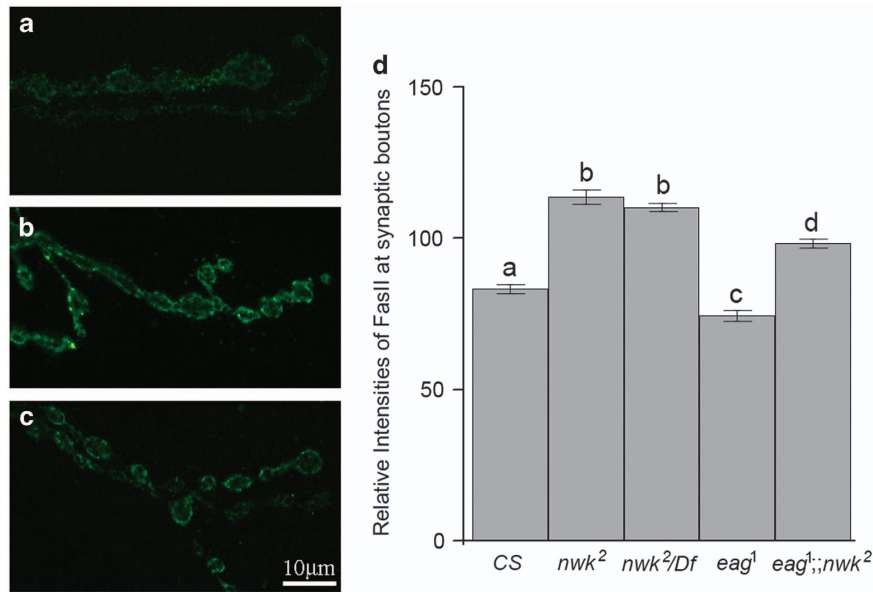
Figure 5 Increased FasII localization at synapses and boutons in *nwk* NMJs. (**a–c**) Single-slice confocal images taken from several synaptic boutons of CS (**a**), *nwk*[2] (**b**) or *nwk*[2]/*Df* (**c**) larval NMJs. Increased FasII levels were observed in *nwk* mutant NMJs (**b** and **c**). Relative intensities of anti-FasII immunoreactivity at synaptic boutons of each genotype are compared (**d**). Characters above error bars indicate groups that are statistically identical.

($6.39 \pm 1.09 \, \mu m^3$) was reduced to <40% that in CS ($17.37 \pm 4.07 \, \mu m^3$) or <50% that in *eag*[1] NMJs ($12.81 \pm 1.3 \, \mu m^3$) (Figure 4g). Compared with *nwk*[2] NMJs, the bouton length and volume in *eag*[1]*;;nwk*[2] NMJs were statistically identical, but the average bouton surface area (length = $2.39 \pm 0.24 \, \mu m$, surface area = $9.74 \pm 1.81 \, \mu m^2$, volume = $3.38 \pm 0.82 \, \mu m^3$, $n = 9$) was not (Figures 4e–g). These results suggested that synaptic boutons in *eag*[1]*;;nwk*[2] might be more spherical compared with the more elliptical boutons in *nwk*[2]. The normal development of sizes and shapes of synaptic boutons required the expression of Nwk.

Reduced synapse areas in nwk[2] and eag[1];;nwk[2] synaptic boutons

Synapses are electron-dense parallel membrane structures usually harboring T-AZs surrounded by SVs at the presynaptic terminals (Figures 4a–d). The area of total synapses in CS ($0.364 \pm 0.022 \, \mu m^2$, $n = 133$) was similar to that in *eag*[1] ($0.383 \pm 0.023 \, \mu m^2$, $n = 113$). In addition, the average total synaptic area was similar in *nwk*[2] ($0.229 \pm 0.015 \, \mu m^2$, $n = 83$) and *eag*[1]*;;nwk*[2] boutons ($0.213 \pm 0.019 \, \mu m^2$, $n = 64$), even though they were significantly smaller than those in CS or *eag*[1] boutons (Figure 4h). Previous studies in synapses in *Drosophila* larval Type 1b boutons suggested that synapses are ever changing structures undergoing emerging, strengthening, maturing, weakening or other processes. Studies in *brp* (*Drosophila* homolog of human active zone protein ELSK/CAST/ERC) loss-of-function mutants showed that T-AZs at synapses were essential for maintaining activity-dependent release of SVs, rather than spontaneous release of SVs.[39,40] These studies suggested that synapses without a T-AZ may be silent, while one or more T-AZs may be

active synapses undergoing activity-dependent SV exocytosis. Therefore, the synapses in each genotype were further divided by the numbers of T-AZs present. In this analysis, 25% of CS synapses, 22% of *nwk*[2] synapses, 18% of *eag*[1] synapses and 34% of *eag*[1]*;;nwk*[2] synapses lacked a T-AZ and were considered silent synapses, while 63% of CS synapses, 65% of *nwk*[2] synapses, 64% of *eag*[1] synapses and 59% of *eag*[1]*;;nwk*[2] synapses were with one T-AZ. In addition, 11% of CS synapses, 12% of *nwk*[2] synapses, 19% of *eag*[1] synapses and 6% of *eag*[1]*;;nwk*[2] synapses had two or more T-AZs. The areas of silent synapses in *nwk*[2] ($0.090 \pm 0.009 \, \mu m^2$) and *eag*[1]*;;nwk*[2] ($0.096 \pm 0.012 \, \mu m^2$) boutons were <50–60% of those in CS ($0.163 \pm 0.017 \, \mu m^2$) and *eag*[1] ($0.187 \pm 0.024 \, \mu m^2$) boutons (Figure 4i). However, the area of synapses with one T-AZ in *eag*[1]*;;nwk*[2] ($0.252 \pm 0.022 \, \mu m^2$) boutons was only significantly different from those in CS ($0.352 \pm 0.02 \, \mu m^2$) or *eag*[1] ($0.348 \pm 0.02 \, \mu m^2$) boutons (Figure 4j). The areas of synapses with one T-AZ in *nwk*[2] ($0.293 \pm 0.022 \, \mu m^2$) were not significantly different from those of CS, *eag*[1] or *eag*[1]*;;nwk*[2]. The areas of synapses with two T-AZs in *nwk*[2] boutons were significantly reduced, to ~60% of those in CS or *eag*[1] boutons (Figure 4k, CS, $0.793 \pm 0.0669 \, \mu m^2$; *nwk*[2]; $0.462 \pm 0.0486 \, \mu m^2$; *eag*[1], $0.709 \pm 0.0663 \, \mu m^2$; *eag*[1]*;;nwk*[2]; $0.482 \pm 0.0989 \, \mu m^2$). These EM morphometry results showed that Nwk has important roles in maintaining synapses at the proper sizes, and they explain why *nwk*[2] mutants showed reduced evoked junctional current in a previous study.[31]

FasII levels at synaptic boutons were increased at nwk NMJs

Another phenotype observed from NMJs in hyperexcitability mutant is decreased FasII localization at boutons.[20] Down-regulation of FasII at boutons by increased neuronal activities,

hypomorphic mutations in *fasII* or activation of mitogen-activated protein kinase-RAS signaling in NMJs resulted in increased numbers of boutons.[46] Given that Nwk acts via a signaling mechanism different from that of canonical Hebbian plasticity, FasII localization at boutons of *nwk*[2] NMJs might be different from those of boutons of *eag*[1] NMJs. Indeed, FasII localization at boutons in *nwk*[2] NMJs was significantly increased compared with boutons in CS or *eag*[1] NMJs (Figures 5a–c). Relative FasII immunoreactivity at the NMJs in *nwk*[2] or *nwk*[2]/*Df* mutants was 120.3 ± 2.6 or 119.4 ± 2.1, respectively, an increase of ~40% compared with those in CS (86.3 ± 1.3). FasII levels in *eag*[1];;*nwk*[2] NMJs (98.3 ± 1.5) were increased by ~30% compared with those in *eag*[1] NMJs (74.4 ± 1.8) and decreased by ~20% compared with those in *nwk*[2] or *nwk*[2]/*Df* (Figure 4d). These adjusted FasII levels in *eag*[1];;*nwk*[2] NMJs reinforced our hypothesis that Nwk is a component of a signaling mechanism that is different from canonical Hebbian plasticity.

Genetic interaction between Nwk and FasII in regulating synaptic morphology
The synaptic bouton number (61.0 ± 3.33) and branch length ($399.6 \pm 17.0\,\mu m$) in *fasII*[e76] NMJs were <50% of those in CS or *nwk*[2] NMJs (Figures 3g1). However, the synaptic boutons of *fasII*[e76] ($13.18 \pm 0.93\,\mu m^2$, $n = 82$) were twice as large as those of CS (Figures 3g2 and k). Further, *fasII*[e76]/+ NMJs expressed FasII protein at ~55% of the level observed in CS NMJs and had similar average numbers of synaptic boutons (141.8 ± 5.64) as *eag*[1] and *nwk*[2] NMJs (Figures 3e1 and i). The branch length and bouton area in *fasII*[e76]/+ NMJs were not significantly different from those of CS or *eag*[1] NMJs (Figures 3e1). These results suggested that reduced FasII at NMJs is enough to induce increased bouton numbers but not sufficient to extend the length of synaptic branches. Increased FasII localization at boutons of *nwk*[2] NMJs (Figure 5) and compensatory localization patterns between Nwk and FasII at boutons of CS NMJs (Figure 1c) suggested that Nwk and FasII may have complementary roles in regulating synaptic plasticity. To gain insight into unknown mechanisms underlying synaptic plasticity by FasII and Nwk, FasII protein levels in *nwk*[2] NMJs were genetically regulated by recombining *fasII*[e76] mutant chromosomes. When FasII expression was reduced to 10% of CS, the numbers of synaptic boutons and bouton midline areas in *fasII*[e76];;*nwk*[2] (118.1 ± 4.22; $729 \pm 0.471\,\mu m^2$, $n = 102$) were not significantly different from those of CS (Figures 3h1). These results suggested that *fasII*[e76] and *nwk*[2] mutations mutually suppressed the opposing phenotypes when 10% of the normal level of FasII was expressed. Only the length of synaptic branches of *fasII*[e76];;*nwk*[2] ($732.8 \pm 40.4\,\mu m$) was similar to those of *nwk*[2] NMJs. When FasII expression was reduced to 55% of CS, the bouton numbers of *fasII*[e76]/+;;*nwk*[2] (132.6 ± 4.73) and *fasII*[e76]/+;;*nwk*[2]/*Df* (131.4 ± 6.92) NMJs were similar to those of *fasII*[e76]/+ and *nwk*[2] mutants (Figures 3f1 and i). However, the synaptic branch lengths of *fasII*[e76]/+;;*nwk*[2] ($781.0 \pm 54.8\,\mu m$) and *fasII*[e76]/+;;*nwk*[2]/*Df* ($821.4 \pm 34.1\,\mu m$) were similar to those of *nwk*[2] mutants. In addition, the bouton midline areas of

fasII[e76]/+;;*nwk*[2] ($6.638 \pm 0.41\,\mu m^2$, $n = 128$) were similar to those of *fasII*[e76]/+ (Figures 3f2 and k).

Our NMJ morphology analysis results suggested that three morphological aspects examined in this study could be regulated by different signaling mechanisms. We can suggest that FasII is downstream of Nwk in regulating the numbers and sizes of synaptic boutons but either is upstream in the regulation of synaptic branch length or does not participate in this process. Further studies with other mutants showing altered morphologies will reveal more details of the signaling mechanisms.

nwk synapses showed impaired RRPs at T-AZs
The localization of Nwk with SVs at the confocal microscopic level (Figure 1) and EM level (Figure 2) suggested that Nwk may have important roles in regulating SV trafficking or transmission. Electrophysiological studies showed that the quantal contents of *nwk*[2] NMJs were ~50% less than those of CS, although the amplitude of miniature excitatory junctional currents or quantal sizes were slightly increased without changes in frequency of miniature excitatory junctional currents.[31] Even though the ~50% decrease in the numbers of synapses and T-AZs in *nwk*[2] boutons may contribute to reduced synaptic transmission in *nwk*[2] NMJs, the numbers of synaptic boutons in *nwk*[2] NMJs were increased by ~40%. These results suggested that other defects caused by loss of Nwk at synaptic terminals may exist. Thus we further examined whether SV pools in *nwk*[2], *eag*[1] or *eag*[1];;*nwk*[2] boutons were altered.

First, we examined whether Mab-Synapsin signals in *nwk*[2] boutons were altered (Figures 6a–d). When *nwk*[2], *eag*[1] or *eag*[1];;*nwk*[2] boutons were compared with CS, only *nwk*[2] boutons appeared to have reduced Synapsin immunoreactivity. *eag*[1] boutons showed stronger signals and *eag*[1];;*nwk*[2] boutons showed signals similar to those of CS. These results suggested that Nwk may be critical for maintaining normal SV pools at the presynaptic terminals.

Next, we examined whether RRP and RP were altered in *nwk*[2] boutons by performing EM (Figures 6e–h). In this study, the RRP and RP were defined as SVs within 200 nm or at 200–400 nm, respectively, from the stub of T-AZs. The numbers of SVs in the RRP (6.44 ± 0.27) or RP (10.83 ± 0.53) in *nwk*[2] were significantly less than those of CS (RRP, 11.49 ± 0.28; RP, 24.115 ± 0.77). The RRPs of *eag*[1] (12.72 ± 0.38) and *eag*[1];;*nwk*[2] (12.43 ± 0.30) were significantly increased compared with that of CS. However, only the RP of *eag*[1] (28.21 ± 0.91) was significantly increased compared with that of CS. The RP of *eag*[1];;*nwk*[2] (23.26 ± 0.82) was similar to that of CS (Figure 6i). These results suggested that Nwk is critical for maintaining the RRP and RP. In addition, the reduction in SVs induced by the loss of Nwk at the presynaptic terminals might be offset by increased neural activity, which is known to strengthen synaptic connections.

Nwk formed a protein complex with DSypt1 and Synapsin
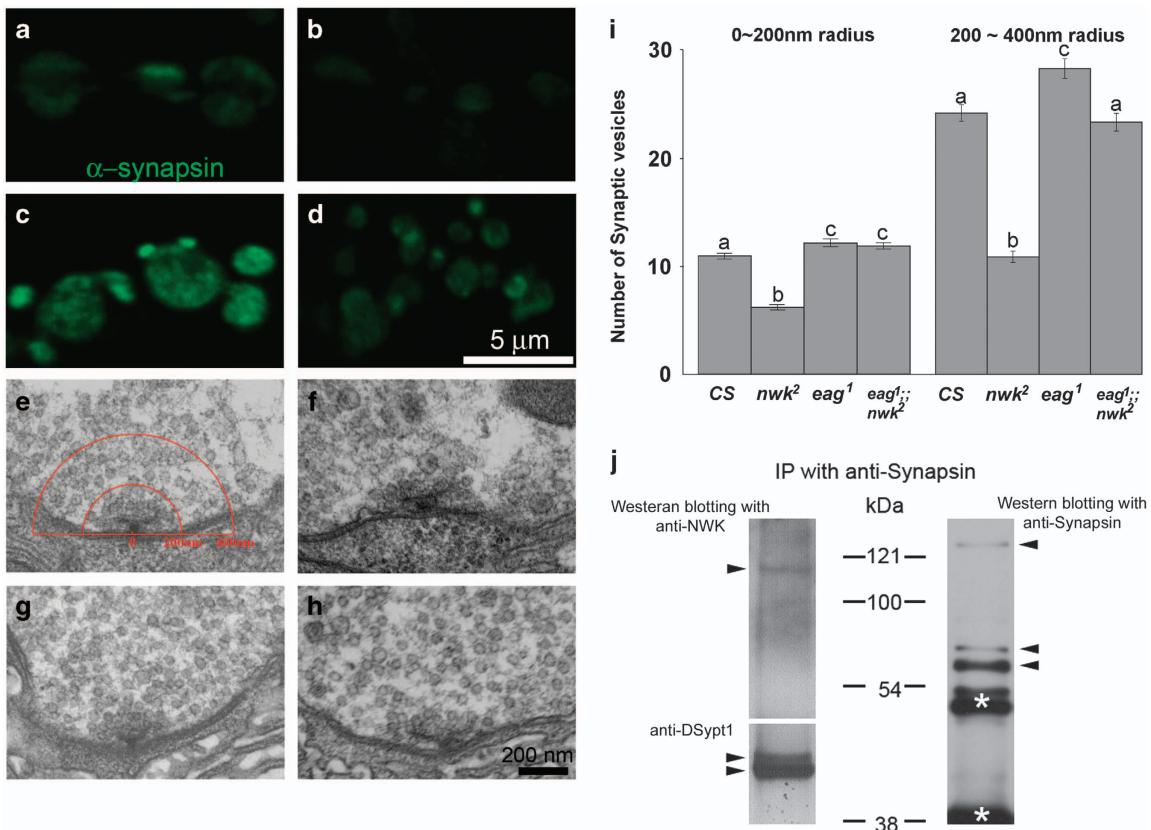Reduced Synapsin immunoreactivities together with reduced RRP and RP at *nwk* mutant synapses suggested that NWK and

Figure 6 Synapsin immunoreactivity and SV numbers were significantly reduced in *nwk²* mutant synaptic boutons. (**a**–**d**) Mab-Synapsin immunoreactivity in *nwk²* mutant synaptic boutons (**b**) appeared to be weaker than CS (**a**), *eag¹* (**c**) or *eag¹;;nwk²*. (**e**–**f**) Ultrastructural analysis of SVs near T-AZs showed fewer SVs in *nwk²* (**f**), *eag¹* (**g**) or *eag¹;;nwk²*(**h**) compared with CS (**d**). (**i**) The SV numbers in RRP (0–200 nm) or RP (200–400 nm) from a T-AZ in *nwk²* mutant synaptic boutons were significantly reduced. (**j**) Mab-Synapsin coprecipitated with Nwk, *D*Sypt1 and Synapsin from protein extracts from larval body wall muscle preparations. Characters above error bars indicate groups that are statistically identical.

Synapsin may present at the same protein complexes. To investigate this possibility, we performed Mab-Synpasin immunoprecipitation and proved precipitates with rabbit anti-Nwk or anti-DSypt1 antibodies (Figure 6j). There were clear one Nwk and two *D*Sypt1 bands when Mab-Synapsin precipitates were separated. Consistent with a previous report,[47] three Synapsin bands were clearly detected. These results suggested that NWK formed a protein complex with *D*Sypt1 and Synapsin and regulates SV trafficking and transmission.

3D HVEM tomography revealed T-AZ architectures of CS and nwk² synapses at high resolution
To investigate SV localization patterns and synaptic architecture at three dimensions, CS and *nwk²* synapses in Type 1b boutons were analyzed by 3D HVEM tomography. Examples of unprocessed HVEM images of CS and *nwk²* synapses are shown in Figures 7a and b. Using 121 tilted images, 3D ultrastructures of synapses (Figures 7c and d) and T-AZs (Figures 7e and f) of CS and *nwk²* were generated by IMOD.[37] Because fewer SVs with enlarged sizes were observed from *nwk²*, we further quantified the 3D distribution patterns of SVs in RRPs. Consistent with conventional EM results (Figures 6e–h), significantly fewer SVs presented at RRP (CS,

138.0 ± 9.0; *nwk²*, 91.0 ± 6.8, $P < 0.01$). The graphs showing SVs numbers based on distances from the stub of T-AZs suggested that no SVs were docked to T-AZs in *nwk²*. However, more SVs localized from 100 to 140 nm from T-AZs in *nwk²* than in CS. In addition, SV size distribution results (Figure 7i) revealed that SVs in *nwk²* were significantly larger than those in CS (*nwk²*, 42.69 ± 0.45; CS, 39.40 ± 0.315 nm, $P < 0.001$). The 3D ultrastructural differences at synapses and T-AZs between CS and *nwk²* were clearly visualized by 3D rotation videos (Supplementary Video Clips 1). Significantly fewer but enlarged SVs were present in the RRPs in *nwk²* synapses.

DISCUSSION
In order to investigate the unknown *in vivo* functions of proteins containing SH3 and F-BAR domains in synaptic plasticity and transmission, we took advantage of *Drosophila* NMJs and available *nwk* mutants. Nwk is a *Drosophila* homolog of MEGAP, one of the proteins responsible for mental retardation in humans; Nwk was initially discovered by temperature-sensitive paralysis behavior of adult flies.[31] Although genetic and physical interactions between Nwk and components of endocytosis, such as Dap160 and Dynamin,[48] and actin cytoskeleton regulators, such as Wiskott–Aldrich
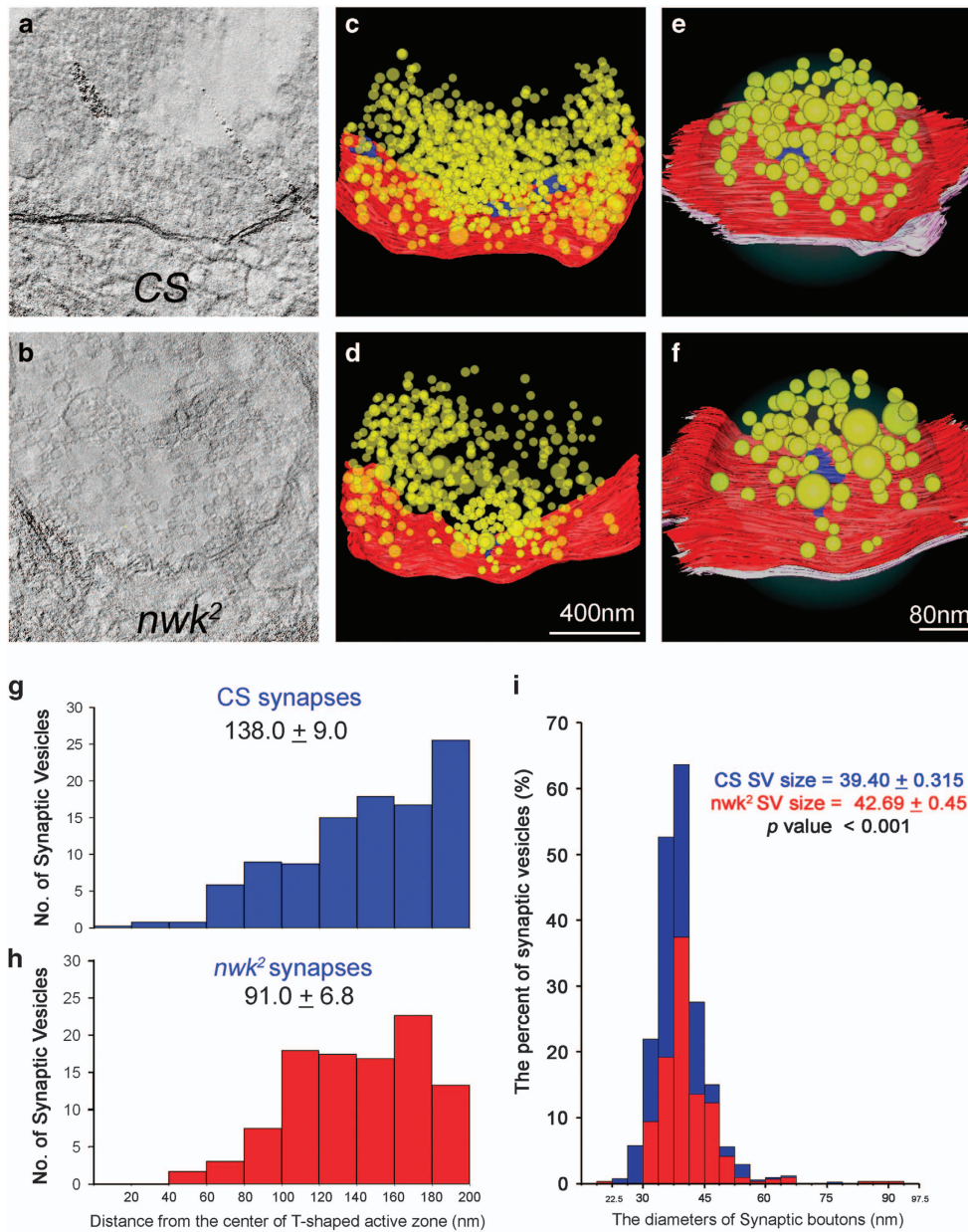
Figure 7 HVEM analysis of *nwk* mutant synapses reinforced altered SV sizes and distribution. Representative HVEM photographs taken from CS (**a**) or *nwk²* (**b**) synapses before processing with IMOD. 3D images of synapses and active zones in CS (**c**) or *nwk²* (**d**). The numbers of SVs from T-AZs in CS (**g**) or *nwk²* (**h**) synapses were quantified. The ratio of SVs in CS (blue) and *nwk²* (red) based on their diameters (**i**) using 400 SVs from CS and 318 SVs from *nwk²*.

syndrome protein[31] and CDC42,[49] have been reported, the localization patterns of Nwk at synaptic boutons appear to be different from localization patterns of the above-mentioned proteins. Thus we hypothesized that Nwk may directly or indirectly interact with other synaptic or cytoskeletal components. In addition, by performing immunohistochemistry to confirm partial colocalization of Nwk with DAP160 (Figure 1j),[48] we also observed via confocal microscopy that Nwk partially colocalized (Figures 1e and f) and formed protein complexes (Figure 6j) with Synapsin and *D*Sypt1. Furthermore, we found that Synapsin immunoreactivities at *nwk* synaptic boutons were significantly reduced (Figures 6a–d). These

findings are highly intriguing because recent studies have shown that Synapsin, the most abundant presynaptic phosphoprotein in *Drosophila*, has a pivotal role in regulating SV trafficking at synaptic terminals by forming protein complexes with Dap160[50] in glutamatergic NMJs. The defects of RRP and RP in *nwk* mutant synapses were further confirmed by performing transmission EM analysis (Figures 6e–i) and HVEM 3D tomography (Figures 7a–i). Thus it is possible that Nwk is actively participating in SV trafficking at RRP and RP via interactions with Synapsin, *D*Sypt1 (Figure 6i), Dap160,[50] Dynamin[48] and other interacting proteins that have yet to be identified.

Another phenotype in *nwk* loss-of-function mutants that was able to be identified by this study's use of HVEM 3D tomography was that of enlarged SVs (Figures 7a–i). Because we used 1 μm thick sections for examining size and distribution of SVs at *nwk* mutant and control synapses and as 20 nm gold particles were used to create a list of fiducial points and size standards for SVs, our HVEM 3D analysis results did not contain biased data originating from measuring diameters of sectioned SVs when 50–100 nm of thin sections were used for conventional transmission EM analysis as described by Kim et al.[51] Recently, it has been shown that an F-BAR domain in Nwk binds to and remodels membranes to form concave membrane structures.[52] Therefore, it is possible that Nwk may regulate SV recycling both directly, by interacting with synaptic membranes, and indirectly, through its binding partners, such as Synapsin, *D*Sypt1, Dap160 and Dynamin. Thus loss of Nwk at synapses might induce enlarged SVs compared with control synapses.

In addition to regulating SV size and trafficking, our NMJ and synapse morphometric analysis results provided several lines of evidence supporting that Nwk regulates synaptic plasticity of glutamatergic NMJs in a manner different from activity-dependent Hebbian plasticity. Previous studies have shown one of the classical examples of Hebbian plasticity, in which increased neuronal activity in NMJs reduces FasII localization at synaptic boutons, resulting in both an increase in the number of synaptic boutons and branch elongation.[19,22] However, the findings of this study, which supported that genetically increased neuronal activity in *nwk*[2] mutant NMJs resulted in significantly more synaptic boutons and branch elongations (Figure 3) and that the levels of FasII in *nwk*[2] mutants were significantly higher than those of CS (Figure 5), suggested that Nwk may exist in a different signaling pathway from that of Hebbian plasticity.

The evidence presented in this study is important because most psychiatric and neurological diseases, ranging from autism and mental retardation to dementia, are reported to be accompanied by altered synaptic structures and functions.[1] The association of MEGAP and mental retardation has been revealed in the process of identifying genes that are linked with distal chromosome 3p deletion syndrome (3p-syndrome) patients with severe mental retardation.[3,53] Similar to Nwk, MEGAP expression was observed in the embryonic central nervous systems of mice[54] and high expression was found in the hippocampus, amygdala, piriform cortex, posterior parietal associative area and the dentate gyrus of adult mouse brains.[3] In addition, similar to Nwk, MEGAP binds strongly to the phosphoinositide-rich membrane and is involved in the formation of filopodia.[52] In the synaptogenesis stage, MEGAP has an important role in synapse selection, and consequently, the loss of MEGAP function results in a decrease in the number of neuron spines.[55] Thus, although it has not been elucidated to date whether MEGAP expresses at presynaptic or postsynaptic terminals or both, it is possible that MEGAP may regulate SV size and distribution in neuron spines at glutamatergic synapses of the mouse central nervous system, especially at the hippocampus, resulting in mental retardation phenotypes in human patients[3] and mouse knockout models.[55,56] Thus further studies in Nwk and MEGAP will reveal unknown molecular and cellular functions of SH3 and F-BAR domain proteins in synaptic plasticity and mental retardation.

CONFLICT OF INTEREST

The authors declare no conflict of interest.

PUBLISHER'S NOTE

Springer Nature remains neutral with regard to jurisdictional claims in published maps and institutional affiliations.

1 van Spronsen M, Hoogenraad CC. Synapse pathology in psychiatric and neurologic disease. *Curr Neurol Neurosci Rep* 2010; **10**: 207–214.

2 Turrigiano GG. The self-tuning neuron: synaptic scaling of excitatory synapses. *Cell* 2008; **135**: 422–435.

3 Endris V, Wogatzky B, Leimer U, Bartsch D, Zatyka M, Latif F et al. The novel Rho-GTPase activating gene MEGAP/ srGAP3 has a putative role in severe mental retardation. *Proc Natl Acad Sci USA* 2002; **99**: 11754–11759.

4 Jin P, Alisch RS, Warren ST. RNA and microRNAs in fragile X mental retardation. *Nat Cell Biol* 2004; **6**: 1048–1053.

5 Gabellini D, Green MR, Tupler R. When enough is enough: genetic diseases associated with transcriptional derepression. *Curr Opin Genet Dev* 2004; **14**: 301–307.

6 Belmonte MK, Allen G, Beckel-Mitchener A, Boulanger LM, Carper RA, Webb SJ. Autism and abnormal development of brain connectivity. *J Neurosci* 2004; **24**: 9228–9231.

7 Fang P, Lev-Lehman E, Tsai TF, Matsuura T, Benton CS, Sutcliffe JS et al. The spectrum of mutations in UBE3A causing Angelman syndrome. *Hum Mol Genet* 1999; **8**: 129–135.

8 Zoghbi HY. Postnatal neurodevelopmental disorders: meeting at the synapse? *Science* 2003; **302**: 826–830.

9 Turrigiano GG, Nelson SB. Homeostatic plasticity in the developing nervous system. *Nat Rev Neurosci* 2004; **5**: 97–107.

10 Vitureira N, Goda Y. The interplay between Hebbian and homeostatic synaptic plasticity. *J Cell Biol* 2013; **203**: 175–186.

11 Toyoizumi T, Kaneko M, Stryker MP, Miller KD. Modeling the dynamic interaction of hebbian and homeostatic plasticity. *Neuron* 2014; **84**: 497–510.

12 Desai NS. Homeostatic plasticity in the CNS: synaptic and intrinsic forms. *J Physiol* 2003; **97**: 391–402.

13 Abbott LF, Regehr WG. Synaptic computation. *Nature* 2004; **431**: 796–803.

14 O'Rourke NA, Weiler NC, Micheva KD, Smith SJ. Deep molecular diversity of mammalian synapses: why it matters and how to measure it. *Nat Rev Neurosci* 2012; **13**: 365–379.

15 Koh YH, Gramates LS, Budnik V. Drosophila larval neuromuscular junction: molecular components and mechanisms underlying synaptic plasticity. *Microsc Res Tech* 2000; **49**: 14–25.

16 Keshishian H. Is synaptic homeostasis just wishful thinking? *Neuron* 2002; **14**: 481–482.

14

17 Packard M, Mathew D, Budnik V. Wnts and TGF-β in synaptogenesis: old friends signaling at new places. *Nat Rev Neurosci* 2003; **4**: 113–120.

18 Koh YH. Drosophila as a model organism for investigating molecular and cellular etiologies underlying complex neurological disorders in humans. *J Asia Pac Entomol* 2006; **9**: 75–84.

19 Budnik V, Zhong Y, Wu CF. Morphological plasticity of motor axons in Drosophila mutants with altered excitability. *J Neurosci* 1990; **10**: 3754–3768.

20 Schuster CM, Davis GW, Fetter RD, Goodman CS. Genetic dissection of structural and functional components of synaptic plasticity. I. Fasciclin II controls synaptic stabilization and growth. *Neuron* 1996; **17**: 641–654.

21 Schuster CM, Davis GW, Fetter RD, Goodman CS. Genetic dissection of structural and functional components of synaptic plasticity. II. Fasciclin II controls presynaptic structural plasticity. *Neuron* 1996; **17**: 655–667.

22 Davis GW, Schuster CM, Goodman CS. Genetic analysis of the mechanisms controlling target selection: target-derived Fasciclin II regulates the pattern of synapse formation. *Neuron* 1996; **19**: 561–573.

23 Ljaschenko D, Ehmann N, Kittel RJ. Hebbian plasticity guides maturation of glutamate receptor fields in vivo. *Cell Rep* 2013; **3**: 1407–1413.

24 Kim E, Sheng M. PDZ domain proteins of synapses. *Nat Rev Neurosci* 2004; **5**: 771–781.

25 Rizzoli SO, Betz WJ. Synaptic vesicle pools. *Nat Rev Neurosci* 2005; **6**: 57–69.

26 Kidokoro Y, Kuromi H, Delgado R, Maureira C, Oliva C, Labarca P. Synaptic vesicle pools and plasticity of synaptic transmission at the Drosophila synapse. *Brain Res Brain Res Rev* 2004; **47**: 18–32.

27 Tejedor FJ, Bokhari A, Rogero O, Gorczyca M, Zhang J, Kim E *et al*. Essential role for dlg in synaptic clustering of Shaker K+ channels in vivo. *J Neurosci* 1997; **17**: 152–159.

28 Koh YH, Popova E, Thomas U, Griffith LC, Budnik V. Regulation of DLG localization at synapses by CaMKII-dependent phosphorylation. *Cell* 1999; **98**: 353–363.

29 Thomas U, Kim E, Kuhlendahl S, Koh YH, Gundelfinger ED, Sheng M *et al*. Synaptic clustering of the cell adhesion molecule fasciclin II by discs-large and its role in the regulation of presynaptic structure. *Neuron* 1997; **19**: 787–799.

30 Paradis S, Sweeney ST, Davis GW. Homeostatic control of presynaptic release is triggered by postsynaptic membrane depolarization. *Neuron* 2001; **30**: 737–749.

31 Coyle I, Koh YH, Lee W-CM, Slind J, Fergestad T, Littleton JT *et al*. Nervous Wreck, an adaptor protein that interacts with WASP, regulates synapse growth in Drosophila. *Neuron* 2004; **41**: 512–534.

32 Kim AY, Seo JB, Kim WT, Choi HJ, Kim S-Y, Morrow G *et al*. The pathogenic human Torsin A in Drosophila activates the unfolded protein response and increases susceptibility to oxidative stress. *BMC Genomics* 2015; **16**: 338.

33 Lee DW, Seo JB, Ganetzky B, Koh YH. ΔFY mutation in human Torsin A induces locomotor disability and aberrant synaptic structures in Drosophila. *Mol Cells* 2009; **27**: 89–97.

34 Zhang B, Koh YH, Beckstead RB, Budnik V, Ganetzky B, Bellen HJ. Synaptic vesicle size and number are regulated by a Clathrin adaptor protein required for endocytosis. *Neuron* 1998; **21**: 1465–1475.

35 Roos J, Kelly RB. Dap160, a neural-specific Eps15 homology and multiple SH3 domain-containing protein that interacts with Drosophila dynamin. *J Biol Chem* 1998; **273**: 19108–19119.

36 Schneider CA, Rasband WS, Eliceiri KW. NIH Image to ImageJ: 25 years of image analysis. *Nat Methods* 2012; **9**: 671–675.

37 Kremer JR, Mastronarde DN, McIntosh JR. Computer visualization of three-dimensional image data using IMOD. *J Struct Biol* 1995; **116**: 71–76.

38 Koh YH, Lehfield K, Ganetzky B. A Drosophila model of early-onset torsion dystonia suggests impairments in transforming growth factor-β signaling. *Hum Mol Genet* 2004; **13**: 2019–2030.

39 Wagh DA, Rasse TM, Asan E, Hofbauer A, Schwenkert I, Durrbeck H *et al*. Bruchpilot, a protein with homology to ELKS/CAST, is required for structural integrity and function of synaptic active zones in Drosophila. *Neuron* 2006; **49**: 833–844.

40 Kittel RJ, Wichmann C, Rasse TM, Fouquet W, Schmidt M, Schmid A *et al*. Bruchpilot promotes active zone assembly, Ca²⁺ channel clustering, and vesicle release. *Science* 2006; **312**: 1051–1054.

41 Koh TW, Verstreken P, Bellen HJ. Dap160/Intersectin acts as a stabilizing scaffold required for synaptic development and vesicle endocytosis. *Neuron* 2004; **43**: 193–205.

42 Roos J, Hummel T, Ng N, Klambt C, Davis GW. Drosophila Futsch regulates synaptic microtubule organization and is necessary for synaptic growth. *Neuron* 2000; **26**: 371–382.

43 Delgado R, Maureira C, Oliva C, Kidokoro Y, Labarca P. Size of vesicle pools, rates of mobilization, and recycling at neuromuscular synapses of a Drosophila mutant, shibire. *Neuron* 2000; **28**: 941–953.

44 Roche JP, Packard MC, Moeckel-Cole S, Budnik V. Regulation of synaptic plasticity and synaptic vesicle dynamics by the PDZ protein Scribble. *J Neurosci* 2002; **22**: 6471–6479.

45 Alabi AA, Tsien RW. Synaptic vesicle pools and dynamics. *Cold Spring Harb Perspect Biol* 2012; **4**: a013680.

46 Koh YH, Ruiz-Canada C, Gorczyca M, Budnik V. The Ras1–mitogen-activated protein kinase signal transduction pathway regulates synaptic plasticity through Fasciclin II-mediated cell adhesion. *J Neurosci* 2002; **22**: 2496–2504.

47 Klagges BR, Heimbeck G, Godenschwege TA, Hofbauer A, Pflugfelder GO, Reifegerste R *et al*. Invertebrate synapsins: a single gene codes for several isoforms in Drosophila. *J Neurosci* 1996; **16**: 3154–3165.

48 O'Connor-Giles KM, Ho LL, Ganetzky B. Nervous wreck interacts with thickveins and the endocytic machinery to attenuate retrograde BMP signaling during synaptic growth. *Neuron* 2008; **58**: 507–518.

49 Rodal AA, Motola-Barnes RN, Littleton JT. Nervous wreck and Cdc42 cooperate to regulate endocytic actin assembly during synaptic growth. *J Neurosci* 2008; **28**: 8316–8325.

50 Winther ÅME, Vorontsova O, Rees KA, Näreoja T, Sopova E, Jiao W *et al*. An endocytic scaffolding protein together with Synapsin regulates synaptic vesicle clustering in the Drosophila neuromuscular junction. *J Neurosci* 2015; **35**: 14756–14770.

51 Kim SJ, Atwoodb HL, Cooper RL. Assessing accurate sizes of synaptic vesicles in nerve terminals. *Brain Res* 2000; **877**: 209–217.

52 Stanishneva-Konovalova TB, Kelley CF, Eskin TL, Messelaar EM, Wasserman SA, Sokolova OS *et al*. Coordinated autoinhibition of F-BAR domain membrane binding and WASp activation by Nervous Wreck. *Proc Nat Acad Sci USA* 2016; **113**: E5552–E5561.

53 Gunnarsson C, Bruun CF. Molecular characterization and clinical features of a patient with an interstitial deletion of 3p25.3-p26.1. *Am J Med Genet A* 2010; **152A**: 3110–3114.

54 Waltereit R, Kautt S, Bartsch D. Expression of MEGAP mRNA during embryonic development. *Gene Expr Patterns* 2008; **8**: 307–310.

55 Carlson BR, Lloyd KE, Kruszewski A, Kim I-H, Rodriguiz RM, Heindel C *et al*. WRP/srGAP3 facilitates the initiation of spine development by an inverse F-BAR domain, and its loss impairs long-term memory. *J Neurosci* 2011; **31**: 2447–2460.

56 Bacon C, Endris V, Andermatt I, Niederkofler V, Waltereit R, Bartsch D *et al*. Evidence for a role of srGAP3 in the positioning of commissural axons within the ventrolateral funiculus of the mouse spinal cord. *PLoS ONE* 2011; **6**: e19887.

Supplementary Information accompanies the paper on Experimental & Molecular Medicine website (http://www.nature.com/emm)